


Improving mechanical and thermal properties of graphite–aluminium composite using Si, SiC and eggshell particles

MO Durowoju¹, TB Asafa¹ , ER Sadiku², S Diouf², MB Shongwe², PA Olubambi², KO Oladosu³, A Ogbemudia¹, MM Babalola¹ and MT Ajala⁴

Journal of Composite Materials
2020, Vol. 54(17) 2365–2376
© The Author(s) 2019
Article reuse guidelines:
sagepub.com/journals-permissions
DOI: 10.1177/0021998319892058
journals.sagepub.com/home/jcm



Abstract

Graphite–aluminium (Gr–Al) composites are being used for diverse engineering applications because of their light weight, good electrical conductivity and thermal properties. However, their applications are limited by high coefficient of thermal expansion and low microhardness values which can be enhanced by adding cheap and efficient fillers. This paper reports the effect of addition of eggshell (ES) particles on the properties of sintered Gr–Al-based composites. Five different composites (Gr–Al, Gr–Al + 20 wt.%Si, Gr–Al + 20 wt.%SiC, Gr–Al + 20Si wt.% + 20 wt.%ES and Gr–Al + 20SiC wt.% + 20 wt.%ES) were sintered at a temperature of 540 °C, holding time of 10 min, heating rate of 52 °C/min and pressure of 50 MPa using spark plasma sintering system. The sintered samples were characterized based on morphology, microhardness, relative density, coefficient of thermal expansion and electrical conductivity. Based on SEM images, graphite particles of flake-like structure were largely undeformed while Al particles were smaller, round and irregular in shape and fairly uniformly distributed in the composites. The microhardness value of sintered Gr–Al + 20 wt.%SiC + 20 wt.%ES composite was 39.55 HV compared to 30.46 HV for Gr–Al, the least of the samples. The Gr–Al + 20 wt.%SiC + 20 wt.%ES composite also has a very low thermal expansion coefficient ($0.98 \times 10^{-5}/K$) but lowest electrical conductivity at temperature beyond 150 °C. Highest densification and minimum relative density (94%) were obtained in Gr–Al + 20 wt.%Si + 20 wt.%ES composite. These enhanced performances are largely due to the incorporation of ES particles. This study therefore demonstrated that ESs particles enhanced microhardness and lowered thermal expansion of Gr–Al-based composites which have promising applications in industries especially for thermal management.

Keywords

Composites, graphite–aluminium, eggshells, silicon particles, sintering

Introduction

In the past few years, several studies have been conducted on graphite–aluminium (Gr–Al) composites because of their diverse engineering applications premised on light weight, good electrical conductivity and low coefficient of thermal expansion (CTE). Gr–Al composites, consisting of graphite infiltrated with aluminium, are largely used for thermal management such as heat sink in high power density electronics¹ and cylinder liners as well as pistons in automobiles.² Hitherto, the problem of bonding between Gr and Al particles was a stumbling block to effective utilization

of the composites. However, several studies were

¹Department of Mechanical Engineering, Ladoko Akintola University of Technology, Nigeria

²Department of Chemical Metallurgical and Materials Engineering, Institute of Nanoengineering Research, Tshwane University of Technology, South Africa

³Department of Mechanical Engineering, Kwara State University, Nigeria

⁴Department of Industrial Maintenance Engineering, Yaba College of Technology, Nigeria

Corresponding author:

TB Asafa, Mechanical Engineering, Ladoko Akintola University of Technology, PMB 4000 Ogbomoso, Ogbomoso, Oyo State 234, Nigeria.
Email: tbasafa@lautech.edu.ng

conducted to enhance the wettability/consolidation leading to adoption of SiO_2 or low melting metals (such as Te, Bi, Pb, Sn, etc.) as binders.³

Prior to this, graphene was added to Al powder in different forms including as nanosheets, nanoplatelets and powder, among others, primarily to enhance strength and heat dissipation. Zhang et al.⁴ used graphene, obtained by reducing graphene oxide, to enhance heat dissipation and mechanical properties of aluminium/graphene composites prepared by powder metallurgy technique. Rashad et al.⁵ utilized graphene nanoplatelets (GNPs) to enhance the mechanical properties of pure aluminium powder using semi-powder manufacturing approach. In this case, Al–0.3wt.% GNPs composite gave higher yield strength, ultimate tensile strength, higher hardness value and lower failure strain compared to monolithic aluminium. Similarly, Li and Xiong⁶ improved the hardness, tensile and ultimate tensile strength of aluminium by adding graphene nanosheets fabricated by high-energy ball milling and vacuum hot pressing. Results also indicated that 0.25wt.% graphene nanosheet gave the optimum mechanical properties while brittle aluminium carbide Al_4C_3 phase was responsible for deterioration of mechanical properties in the post optimal concentration. Furthermore, Huang et al.¹ fabricated graphite film/aluminium composites by vacuum hot pressing and concluded that the composites possess higher in-plane thermal conductivities than graphite flake/aluminium composites due to well-controlled graphite orientation and fabrication parameters.

While most mechanical properties of Gr–Al composites were significantly enhanced by adding graphite/graphene, the major drawbacks are the relatively high CTE, low microhardness value and high relative density (R.D.). To minimize these deficiencies, several studies have been conducted in which fillers were added to Gr–Al powder. However, most of the studies did not optimize all the required properties of the resulting composites. For instance, Durowoju et al.² incorporated micron- and nano-sized ZrB_2 in Gr–Al using spark plasma sintering process. The results indicated that, at high heating rate, the particles promoted densification with slightly improved hardness but raised CTE. This makes the composites less suitable for applications where low CTE is required (especially in thermal management). In a similar work,⁷ Si/SiC particles were used as fillers, and results showed that while SiC lowered densification of Gr–Al powder, addition of 10wt.% silicon marginally increased CTE. These results indicate that the door is still open in search of suitable materials for lowering CTE and improving hardness. In this study, eggshells (ESs) particles, being a low cost reinforcement, lightweight and renewable material, were added to Gr–Al-based composite.

Chicken ES is available abundantly as a by-product of poultry which in most cases are considered as waste, and its disposal constitutes a severe environmental challenge.⁸ ES is attracting attention as a new engineering reinforcement due to its excellent properties such as low density, being renewable, eco-friendliness and high thermal stability. In term of chemical composition, ES contains about 95% calcium carbonate in the form of calcite and 5% organic materials such as Al_2O_3 , SiO_2 , S, CL, P, Cr_2O_3 and MnO .⁹ Studies have shown that the mechanical properties of ESs are enhanced when the calcite crystals are smaller and less mutually aligned.⁹ Consequently, ES had been used to modify mechanical and thermal properties of composites in the past. Hassan and Aigbodion¹⁰ enhanced the performance of Al–Cu–Mg by adding ES at varying proportion. The results revealed that at 12wt.% uncarbonized ES, the tensile strength and the hardness values increased by 8.16% and 10%, respectively, while density and impact energy decreased by 6.5% and 23.5%, respectively. These enhanced strength and hardness values are attributed to the distribution of hard phases of the ES particles in the ductile Al–Cu–Mg alloy matrix.

In another report, Chaithanyasai et al.¹¹ incorporated ES powder into Al 6061 alloy powder, and the results indicated 14% enhanced hardness and reduction in the density of the composite. Also, the mechanical properties of low-density polyethylene,¹² coconut coir fibre,¹³ epoxy,¹⁴ high density polyethylene¹⁵ and polyester¹⁶ among others have been significantly enhanced by adding ES powder.

Several manufacturing processes have been to synthesize composites materials into near net shape. Among the commonly used techniques are solid-state sintering, hot press and spark plasma sintering (SPS). Sintering is a process of compacting and forming (consolidation) a solid mass of material from powders by heat or pressure without melting. It is often conducted at temperature between 65–85% of the powder's melting point in a protective environment. The general driving forces in these techniques is surface tension, external pressure, chemical potential, concentration gradient in multicomponent systems among others.¹⁷ SPS or field-assisted sintering or pulse electric current sintering is preferred over other techniques for many reasons. Additional driving forces (electromechanical stress and high local temperature gradients) create thermal stresses that intensify thermal diffusion and dislocation creep¹⁸ which are responsible for much faster transport mechanisms that accelerate rapid sintering. This also enhances densification for both conductive and nonconductive powder and consequently minimizes grain growth. The process, therefore, takes place within a short time making it an energy and time-saving

technology. SPS consolidates samples by pressure in such a way that a pulsed direct electric current passes through a sample compressed in a graphite die. The process generates local electric discharge plasma and combines the effect of force and electric field. It however causes large temperature gradients due to rapid and non-uniform heating and cooling throughout the sample. So the selection of SPS is largely based on economic consideration.

This paper therefore seeks to incorporate ES particles into Gr–Al-based composite, and then examine how they influence the mechanical and thermal properties of the resulting composites synthesized by SPS technique.

Experimental procedure

Gr–Al powder (average particle size – 80 μm) and silicon powder (size – 45 μm) were purchased from Element Six Production PTY Ltd Company and Alfa Aesar, respectively, while silicon carbide particles (average size – 50 μm) were purchased from Carborundum Co. Ltd, Trafford Park, Manchester. ESs, obtained from Ladoke Akintola University of Technology, Ogbomoso Oyo State, Nigeria, were ball-milled at 250 r/min for 1 h to produce 50 μm size uncarbonized powder. Gr–Al powder was then mixed with 20 wt.%Si, 20 wt.%Si + 20 wt.%ES, 20 wt.%SiC + 20 wt.%ES and 20 wt.%SiC using T2F tubular mixer. To ensure homogenous mixture and significantly reduce temperature heterogeneity, a plastic bottle containing tungsten carbide balls, at a ball to powder ratio of 5:2, was added while the mixer rotated at 100 r/min for 1 h. The blended mixtures were sintered at a temperature of 540 $^{\circ}\text{C}$, holding time of 10 min and heating rate of 52 $^{\circ}\text{C}/\text{min}$ in HHPD25 SPS system (manufactured by FCT Germany). For easy removal, graphite foil of 0.2 mm thickness was inserted between the die and the powder and also between the punch and the powder. In addition, the outer part of the die was covered with a \sim 10 mm thick porous graphite foil as thermal insulator.

To achieve full densification of Gr–Al powder, a sintering temperature of 540 $^{\circ}\text{C}$ was considered following Durowoju et al.⁷ The sintering furnace was maintained at 1 mbar during consolidation while uniaxial pressure of 50 MPa was applied to produce 30 mm diameter discs of the blended powder. The temperature of the sample was monitored with a pyrometer attached to the top of the die at 5 mm from the surface. The linear shrinkage of the powder compact was measured as displacement and displacement rate based on the relative displacement of the graphite punch. CTE was then calculated from the linear shrinkage using
$$CTE = \left(\frac{\epsilon_{T_{room}} - \epsilon_{T_{max}}}{T_{room} - T_{max}} \times \frac{1}{100} \right)^{19-21}$$
 where $\epsilon_{T_{room}}$ and $\epsilon_{T_{max}}$ are linear shrinkages at the end of the cooling and

dwelling process, respectively, while T_{room} and T_{max} are the temperatures at the end of the cooling dwell process, respectively.

The electrical resistivity of the powder was measured with Si_3N_4 non-conducting die and molybdenum punch with 30 mm diameter, 5 mm thick copper base disc. Contacts between the discs and the powders were created by applying a compressive force of 10 kN using power of 8 kW. After the temperature of the powder was stabilized, the power was then increased by 2 kW for every 2 min. The process was halted when the displacement rate started increasing indicating commencement of sintering. The electrical conductivity was then calculated as inverse of electrical resistivity. In addition, the instantaneous R.D., D_i , of the sintered samples was calculated from $D_i = D_f \left(\frac{h_f}{h_i} \right)^{22}$ where D_f is the final R.D. of the sample obtained by the use of Archimedes' principle, and h_f and h_i are the final and instantaneous heights of the samples, respectively. The R.D. was recorded as the arithmetic mean of three different measurements taken from the same sample.

The ratio of the peak intensity of the second highest to the first highest peak intensity of the metal portion of the sintered samples was evaluated from the Peak intensity ratio = $\frac{\text{Intensity of second peak}}{\text{Intensity of first peak}} \times 100\%$.²³ In cases where thermal conductivity experiment cannot be conducted, this ratio has been used to predict the relative thermal conductivities of the chosen composite samples.^{2,24} The intensities of the peaks of the metallic element in the composite samples are extracted, and the peak ratio calculated. The higher the peak intensity ratio, the greater the thermal conductivity. The morphology and phase of the powders and the sintered samples were analyzed using a High Resolution Field Emission Scanning Electron Microscope (JEOL JSM-7600F) with an inbuilt EDX detector (Oxford X-Max) at suitable operating conditions. The microhardness was measured using Vickers indentation method at a load of 100 gf and a dwell time of 15 s. The test results reported are the arithmetic means, with standard deviations, of five successive indentations.

Results and discussion

Morphology of the powders

The morphology and the particle size distribution of the as-received powder and the mixtures are shown in Figure 1. The graphite has large undeformed particles of flake-like structure while Al particles are smaller, round and irregular in shape and fairly uniformly distributed in the composite (Figure 1a). Si powder is largely irregular with size of 45 μm (Figure 1b). The as-received SiC powder is largely irregular with size in the

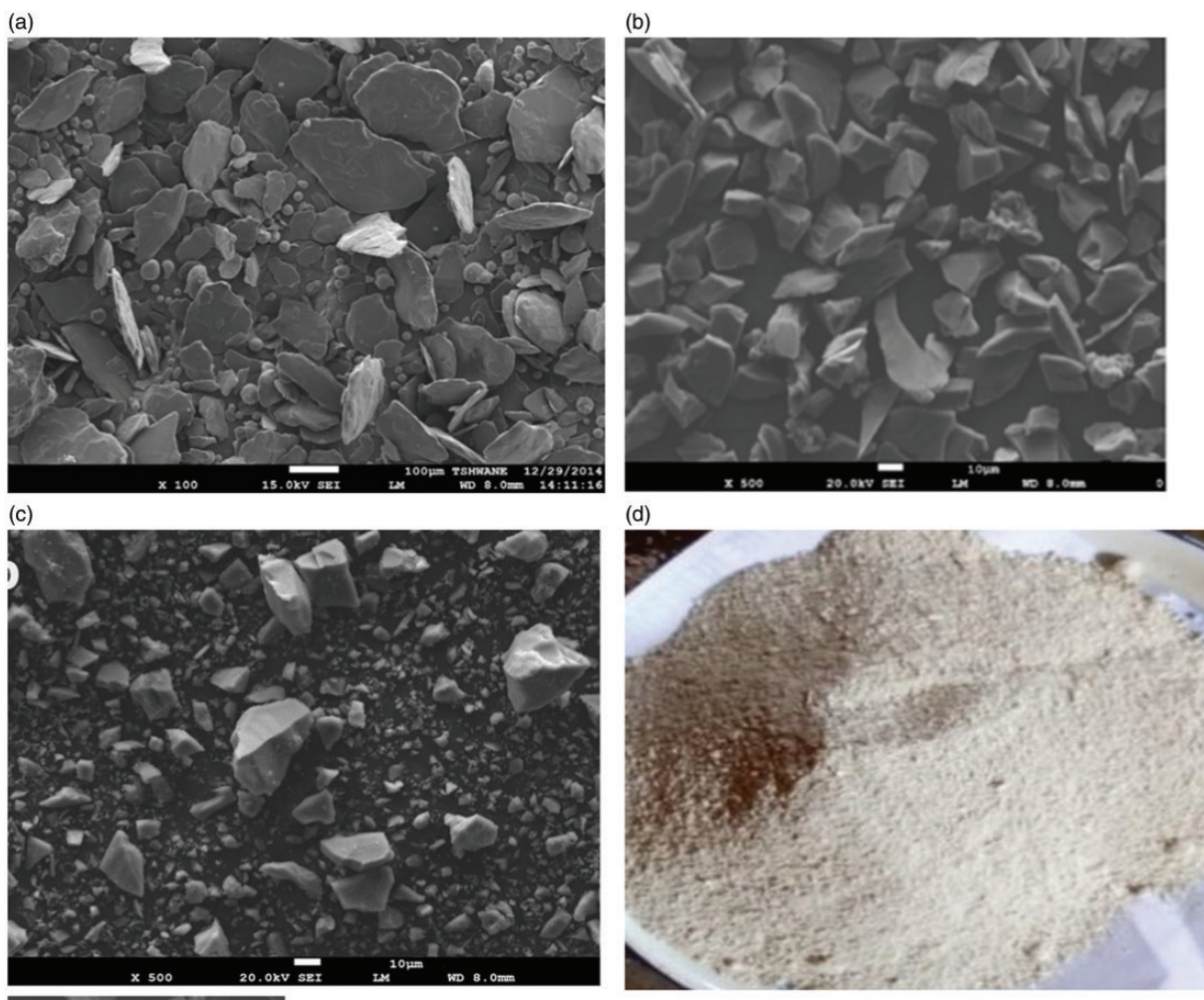


Figure 1. SEM micrographs of (a) Gr–Al, (b) Si and (c) SiC. Ordinary image of uncarbonized eggshells is shown in (d). Gr–Al: graphite–aluminium.

range of 20–50 μm (Figure 1c). The ordinary image of ES powder is shown in Figure 1(d). Previous study² showed that Gr–Al powder contains oxygen (12.9wt.%) which is an indication that the powder is susceptible to oxidation. So, all the mixtures/composites are therefore expected to contain oxygen. The presence of oxygen is expected to enhance oxidation of Si to SiO_2 which served as a wetting agent at the graphite/graphite and graphite/metal interfaces.²

Displacement and densification characteristics

The variation in displacement and temperature against time for all the samples sintered at 540 $^{\circ}\text{C}$ at heating rate of 52 $^{\circ}\text{C}/\text{min}$ is shown in Figure 2 (a) and (b). It is obvious that addition of Si to Gr–Al reduced the displacement of the composites. It can be seen that ES further decreased the displacements

of both Gr–Al + 20 wt.%Si + 20 wt.%ES and Gr–Al + 20 wt.%SiC + 20 wt.%ES composites implying that ES significantly reduced densification. Si and SiC powder, being smaller in size than Gr–Al powder, can occupy the space between Gr–Gr or Gr–Al spacings, and thus, strengthen the resulting composite. In addition, the hard nature of calcite (the major constituent of ES) can lower densification by reducing the displacement rate. It is also interesting to note that the time at which densification commenced decreases with addition of fillers. Densification commenced after 8 min of sintering for Gr–Al + 20 wt.%SiC + 20 wt.%ES compared to 12 min for Gr–Al + 20 wt.%SiC and 11 min for Gr–Al powders. In addition, densification is minimal in Gr–Al + 20Si + 20ES composite than others.

Figure 2(c) shows the variation of displacement rate against time. While Diouf and Molinari²⁵ observed

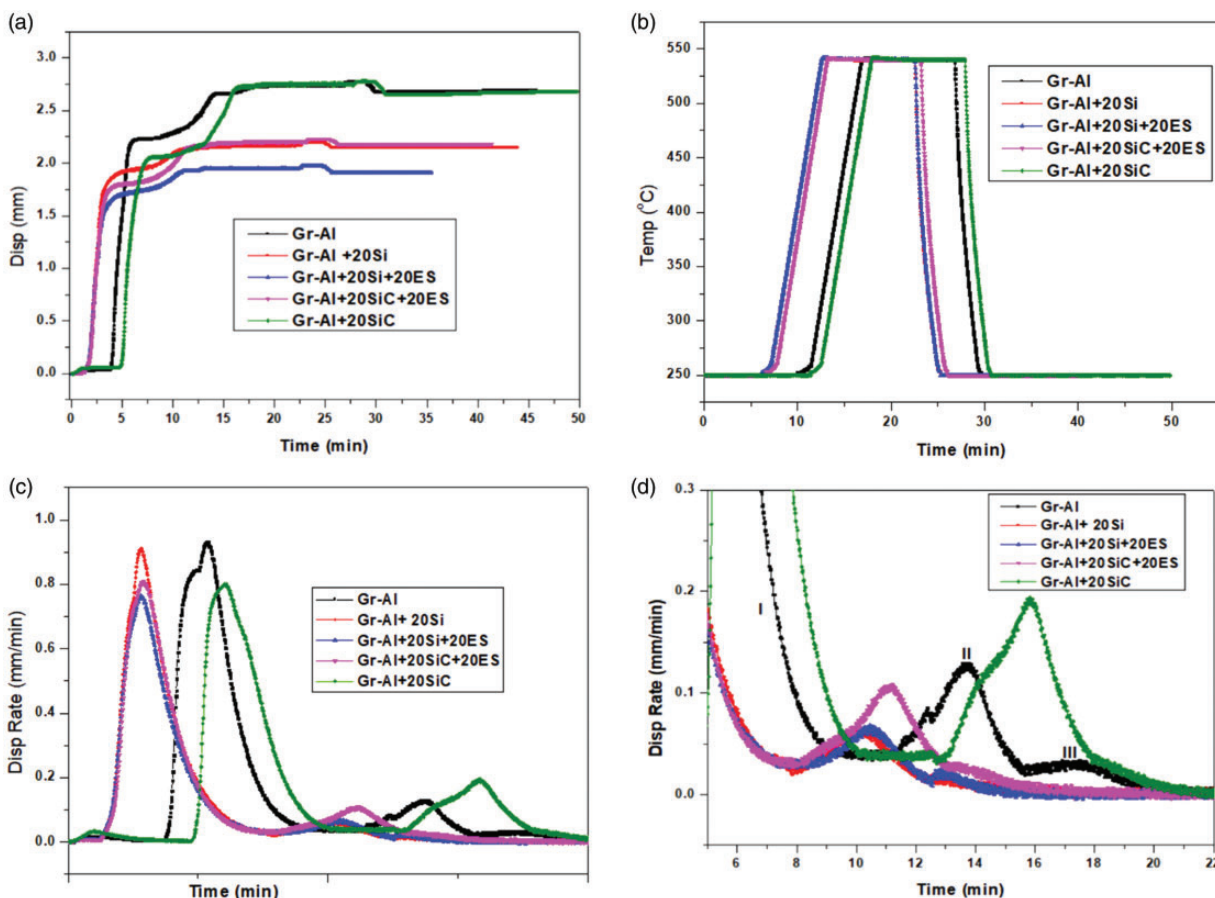


Figure 2. (a) Variation of displacement with time at a sintering temperature of 540°C and heating rate 52°C/min, (b) variation of temperature with time, (c) displacement rate and (d) enlargement of displacement rate to show sintering stages. Gr-Al: graphite-aluminium.

four peaks during densification, three peaks were observed in most of the reported studies thereafter.^{2,7} These peaks are attributed to the phenomenal changes during densification which are rearrangement of powder particles due to the initial pressure, localized deformation, bulk deformation and extensive sintering by mass transport phenomenon. In our case, three distinct peaks are observed for all the samples, implying that the particle rearrangement and localized deformation stages overlapped^{2,7} while other stages occurred in the given sequence. The peak displacement rate also shifted leftwards from Gr-Al except for Gr-Al+20 wt.%SiC corroborating commencement of densification discussed earlier. In another study, Rodriguez et al.²⁶ attributed the slight deviation in the curve patterns of other samples from that of Gr-Al composite to the presence of Si which tends to lower fabrication temperature. The peaks of the displacement rates of Gr+Al+20 wt.%SiC+20 wt.%ES and Gr+Al+20 wt.%SiC occur at 11 min and 16 min, respectively. The 5 min delay in the sintering process may be attributed to the absence of ES particles in

Gr+Al+20 wt.%SiC sample which is known to reduce densification temperature because of its lower melting point compared to SiC.

R.D. and porosity of the samples

The R.D. of Gr-Al+20 wt.%Si decreases slightly compared to that of Gr-Al (Figure 3a). This is attributed to the addition of Si, which has been reported to reduce R.D. when added to Al-based composites.^{7,27} Furthermore, the R.D. of Gr-Al+20 wt.%Si+20 wt.%ES marginally decreases further due to addition of both silicon and ES (which also contains Si). Similarly, addition of ES reduced the R.D. of Gr-Al+20 wt.%SiC. This observation is similar to the finding of Chaithanyasai et al.²⁸ who reported a slight reduction in the density of Al 6061 when ESs were added at varying percentage. Similarly, Hassan and Aigbodion¹⁰ observed slight decrease in density when ESs were added to Al-Cu-Mg alloy. This implies that low-weight composites can be made by adding ESs, Si or SiC as fillers. Such materials are desirable for low-

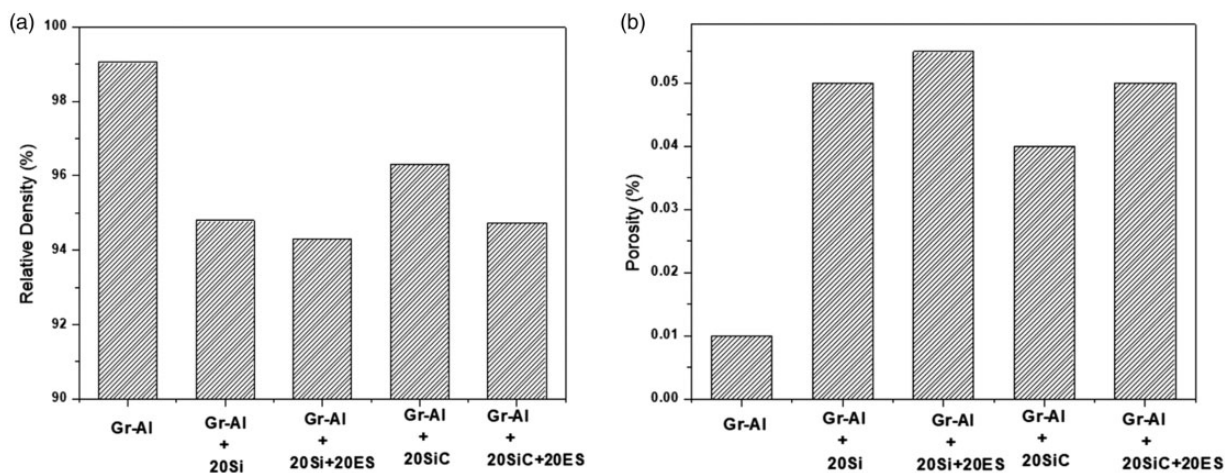


Figure 3. (a) Relative density and (b) porosity of the samples.

Table 1. EDX analysis of the samples (values are in weight percentage).

Elements	Gr-Al	Gr-Al + 20 wt.%Si	Gr-Al + 20 wt.%Si + 20 wt.%ES	Gr-Al + 20 wt.%SiC + 20 wt.%ES	Gr-Al + 20 wt.%SiC
C	82.29	49.72	33.83	83.54	53.60
O	6.78	27.78	22.47	9.70	15.52
Mg	0.09	0.68	0.68	–	–
Al	9.22	3.44	32.36	2.62	27.61
Si	1.34	16.93	9.05	2.48	2.15
K	–	0.66	0.44	–	–
Ca	–	0.11	0.31	1.32	1.11
Fe	0.28	0.67	2.86	0.33	–
Total	100.0	100.0	100.0	100	100

weight devices and automobiles. Meanwhile, addition of Si, SiC and ES lowers the R.D. of Gr–Al more than ZrB₂^{2,7} and thus more effective toward producing low-weight composites.

The reduction in the R.D. can also be justified by the increased porosity of the samples with addition of Si or SiC and ES (Figure 3b). According to the EDX results (Table 1 is based on Figure 4), more oxygen is present in Gr–Al + 20 wt.%Si (~27 wt.%) and Gr–Al + 20 wt.%Si + 20 wt.%ES (~22 wt.%) composites and others compared to Gr–Al (~7 wt.%) composite. Since oxides of metals are less dense than the actual metals, Gr–Al composite is thus expected to be denser than others. Moreover, more volume of oxygen is likely to produce more pores within the microstructure justifying higher porosity observed. This is in agreement with the result reported by Durowoju et al. that porosity increased with the addition of 10wt.% Si to Gr–Al at a sintering temperature of 500 °C. The large amount of oxygen in ES might be responsible for oxide

formation. Consequently, Gr–Al has lower density than others. Figure 4 is an example of SEM micrograph showing EDX region and the corresponding EDX spectrum.

Electrical conductivity

Figure 5 shows that electrical conductivity of the samples increased with temperature. The electrical conductivity of the composites decreases with addition of more fillers (Figure 5a and b). In this case, Gr–Al composite has higher electrical conductivity than others. The decrease in the electrical conductivity is largely due to the reduction in the graphite content as other fillers are added. Knowing fully well that graphite is more conducting than Si, SiC and ES (the electrical conductivity for Gr is 2×10^5 S/m compared to 1.56×10^{-3} S/m for Si), its reduction is expected to lower electrical conductivity of the resulting composites.^{29,30} Generally ES, with calcium carbonate as the major component, is a

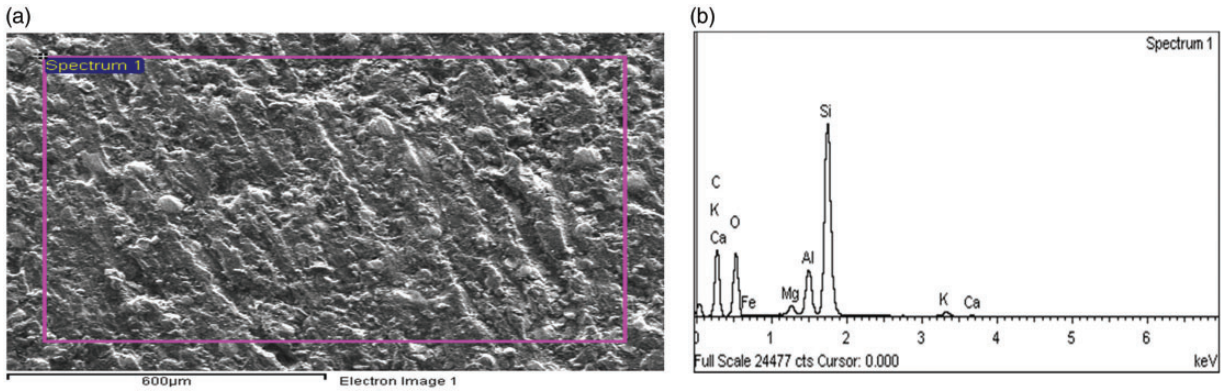


Figure 4. (a) SEM micrograph showing EDX region and (b) EDX spectrum for Gr–Al + 20 wt.%Si + 20 wt.%ES composite.

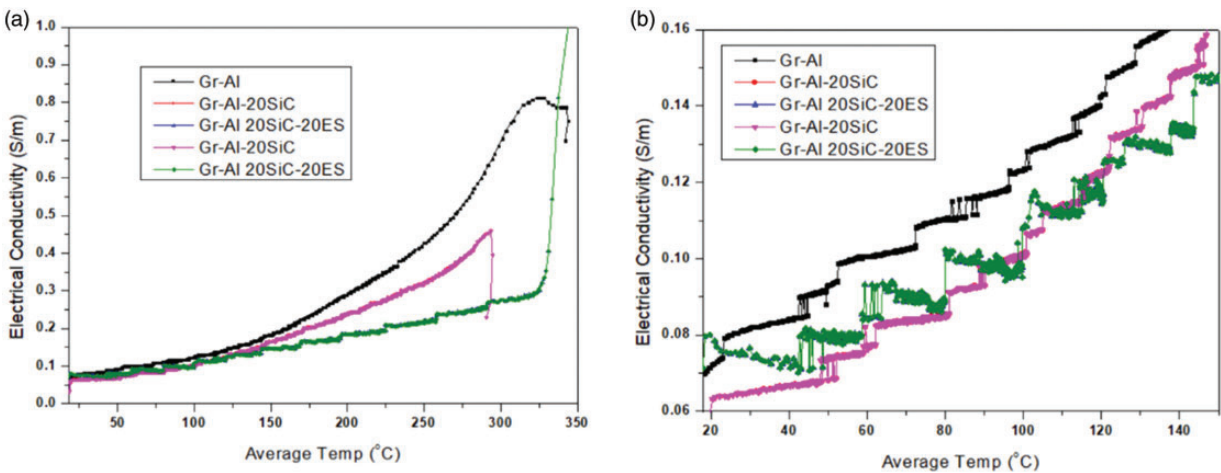


Figure 5. Electrical conductivity as influenced by oven temperature for (a) full range of heating temperature and (b) heating temperature below 140 °C.

Gr–Al: graphite–aluminium.

poor conductor of electricity at room temperature, so its inclusion is expected to lower electrical conductivity of the composite. Chaithanyasai et al.¹¹ also reported a marginal decrease in electrical conductivity when 5wt.%, 10wt.% and 15wt.% ESs were added to aluminium 6061. The decrease in electrical conductivity of the composite is not significant for thermal management which is the target application of this work.

Meanwhile, it is noteworthy that higher porosity is expected to lower electrical conductivity since it weakens electrical pathway. The increase in electrical conductivity with instantaneous R.D. for all the samples is also geometric. For instance, within 5% increase in instantaneous R.D., the electrical conductivity doubles (from 0.06 to 0.12 $\Omega^{-1}\text{m}^{-1}$) implying high dependence. Below 140 °C, the electrical conductivities are not significantly different (Figure 5b). Above this temperature, however, the effect of thermal excitation for improving electrical conductivity is obvious.

Microhardness and CTE

The influence of additional fillers on the microhardness values of the sintered samples is shown in Figure 6. The average hardness values slightly increased from 30.45 ± 3.56 HV for Gr–Al to 32.98 ± 1.48 HV for Gr–Al + 20 wt.%Si and then 33.48 ± 3.29 HV for Gr–Al + 20 wt.%Si + 20 wt.%ES. The highest value of hardness (39.55 ± 4.56 HV) was obtained for Gr–Al + 20 wt.%SiC + 20 wt.%ES composite which is about 7.0 HV higher than that of Gr–Al + 20 wt.%SiC. The results showed that addition of ES enhanced the hardness of Gr–Al + 20 wt.%SiC more than Gr–Al + 20 wt.%Si composite. It appears that the interaction between calcite and SiC leads to the formation of hardened compound such as $\text{CaO}(\text{Al}_2\text{O}_3)$ and AlSiO (see XRD spectra of Figure 8). Si, SiC and ES particles also increase the dislocation density at the particles–matrix interfaces

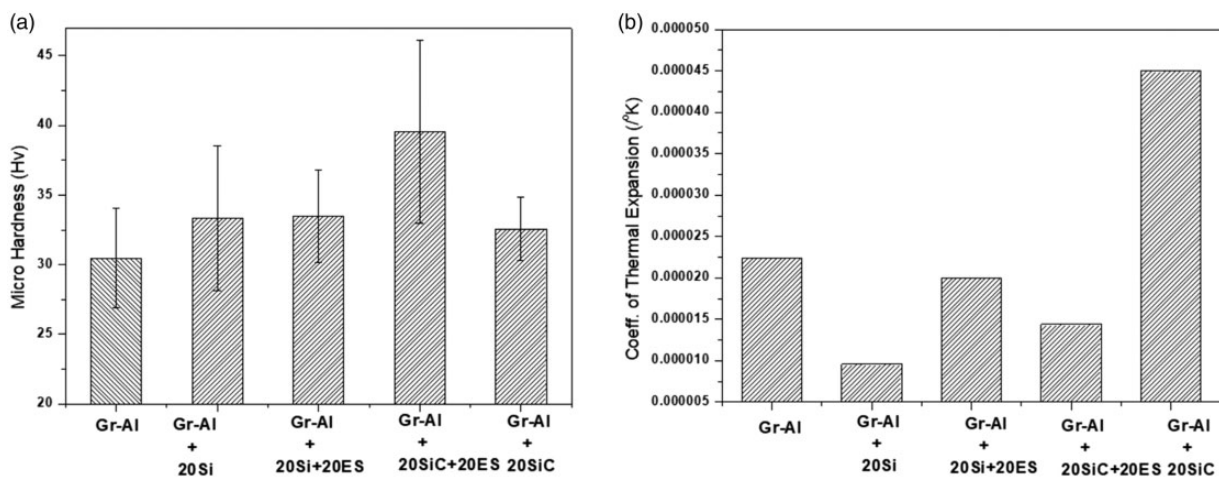


Figure 6. (a) Microhardness values and (b) coefficient of thermal expansion of the samples. Gr-Al: graphite-aluminium.

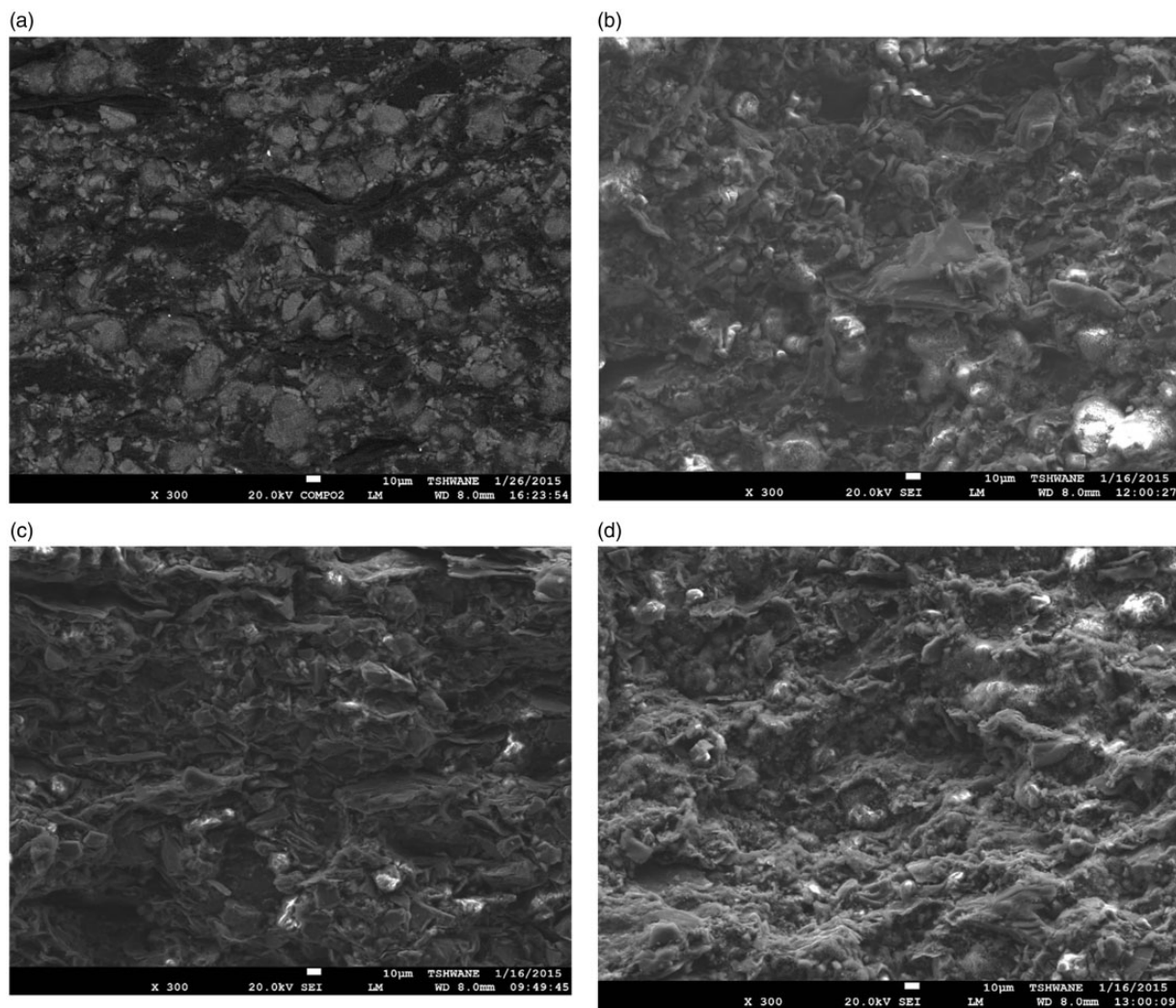


Figure 7. SEM images of sintered Gr-Al reinforced with (a) 20 wt.%Si, (b) 20 wt.%Si + 20 wt.%ES, (c) 20 wt.%SiC and (d) 20 wt.%SiC + 20 wt.%ES.

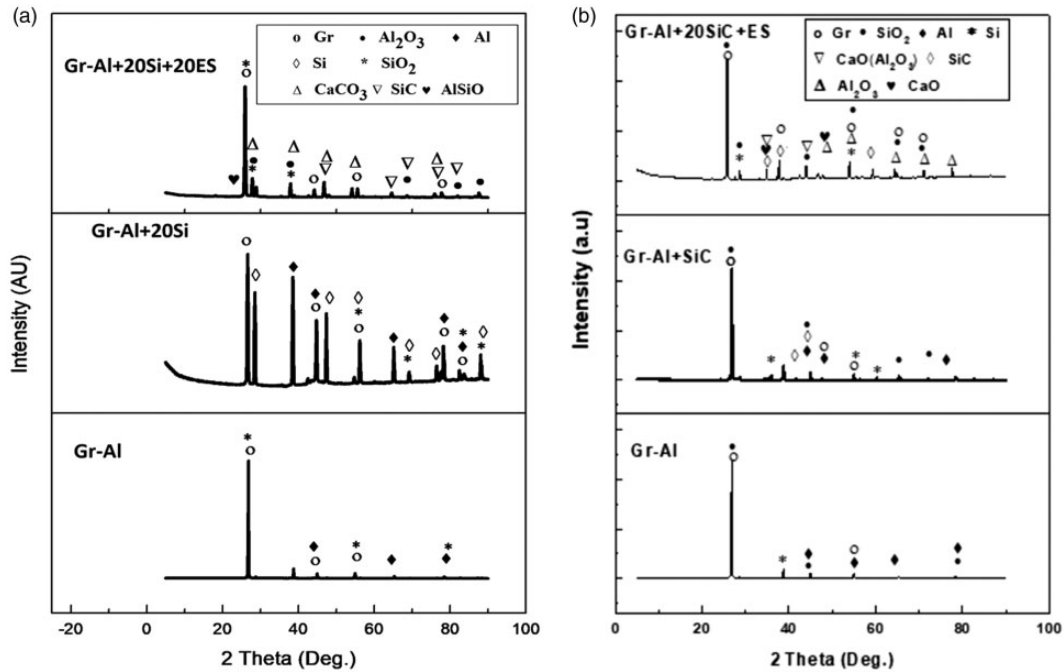


Figure 8. XRD spectral of the sintered samples of Gr–Al modified with (a) Si and ES and (b) SiC and ES.

(due to difference in CTE) which directly enhances hardness.¹⁰ ES particles are more effective than ZrB₂ as fillers in Gr–Al matrix since the latter marginally increased microhardness value by 4%.⁷

The variation in CTE of the sintered samples is presented in Figure 6(b). With addition of 20 wt.%Si to Gr–Al, the CTE decreased by about 50%. This huge reduction in CTE is most likely due to the low CTE of Si ($2.56 \times 10^{-6}/\text{K}$).³⁰ However, upon addition of ES to the composite, the CTE increased close to that of Gr–Al composite. This is because the CTE of ES is higher ($5.4 \times 10^{-6}/\text{K}$)³¹ than that of Si. However, addition of ES to Gr–Al+20 wt.%SiC significantly reduced the thermal conductivity of Gr–Al+20 wt.%SiC by three folds. These results imply that Gr–Al+20 wt.%Si and Gr–Al+20 wt.%SiC+20 wt.%ES composites are more useful than others when low CTE is desired, a major objective of producing composites for thermal management. Similar to ZrB₂, SiC (without ES particles) increased CTE,² and therefore, not useful when lower CTE is desirable.

Microstructure and phase analysis

Figure 7 shows the microstructure of the sintered Al–Gr samples reinforced with different fillers. SEM micrograph of Gr–Al showed some pores which might be due to insufficient densification, melting of the binder and the oxide layer.⁷ All particles were deformed indicating complete sintering at 540°C. Figure 7(a) showed the

SEM micrograph of Gr–Al+20 wt.%Si. It can be seen that graphite particles are of flake like structure while Al particles are round and irregular with random distribution within the graphite particles. Si particles are of irregular shape and distributed randomly in the composite. The microstructure of the sintered Gr–Al+20 wt.%Si+20 wt.%ES samples showed that the particles of ES and Si are evenly distributed in the composite with formation of some pores attributed to the ceramic nature of ES. These pores could be responsible for the high porosity observed in the sample as reported earlier.

The XRD spectral of the phases present in the sintered samples are shown in Figure 8. The spectral confirmed the major constituents as presented in the EDX spectra (Table 1). More peaks appear with addition of Si, SiC and ES to Gr–Al. Silicon appears as a trace in Gr–Al composite, and so also oxygen. This is probably why SiO₂ is hardly observed in Gr–Al compared to other composites where the fraction of Si and oxygen is significant (Table 1). As expected, Ca is observed in Gr–Al+20 wt.%Si+20 wt.%ES and Gr–Al+20 wt.%SiC+20 wt.%ES composite only. Ca is obtained from ES in the form of calcite (CaCO₃). It constitutes 40% of calcite which in turn is made up of 95% of the ES. Since the fraction of the ES in the composite is 20 wt.%, the fraction of Ca obtained is not out of order. No complex or intermetallic compound is observed in the composite.

Furthermore, a significant increase in the peak intensity, compared to the composites without ES, is

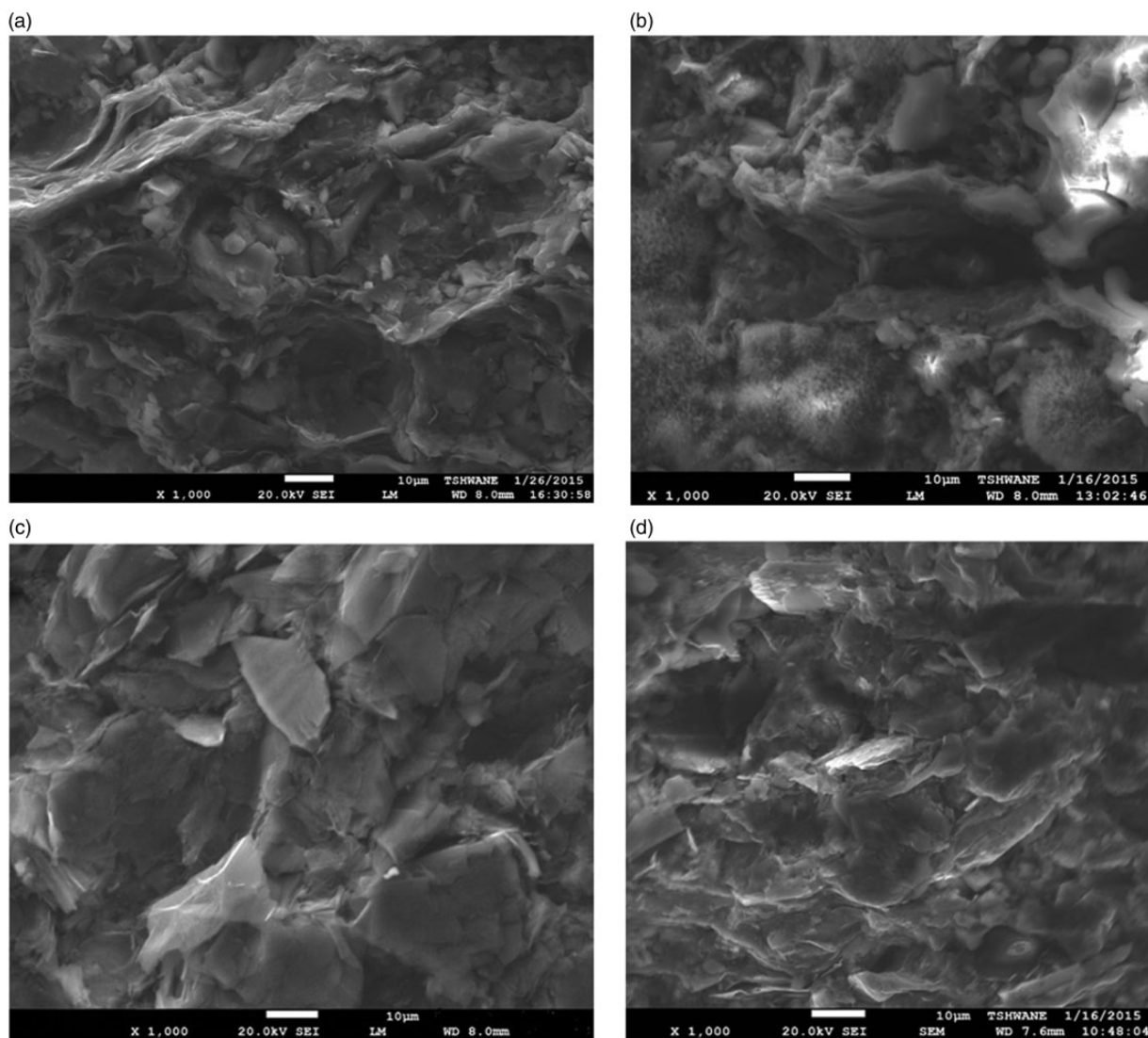


Figure 9. Fracture surfaces of sintered Gr–Al reinforced with (a) 20 wt.%Si, (b) 20 wt.%Si + 20 wt.%ES, (c) 20 wt.%SiC and (d) 20 wt.%SiC + 20 wt.%ES.

Table 2. Peak intensity of the sintered composites.

Samples	First peak intensity	Second peak intensity	Ratio of peak intensity (%)
Gr–Al	34,902	16,615	47.60
Gr–Al+20%Si	7740	4753	61.40
Gr–Al-20%Si+20%ES	9430	1540	16.44
Gr–Al-20%SiC+20%ES	36,324	671	1.84
Gr–Al+20%SiC	43,580	20,425	46.88

observed. It is noteworthy that the ratio of peak intensity of the second highest to the first highest peak intensity of a metal portion can be used to predict the

relative thermal conductivity of composites.²³ In this case, Al is the metal portion, and so data for its peak intensities were extracted from the XRD spectra. These data and the peak intensity ratio are presented in Table 2. As can be seen, the ratio of the peak intensity has the highest value for Gr–Al + 20%Si and the lowest for Gr–Al + 20%SiC + 20 wt.%ES composite. This implies that the thermal conductivity of Gr–Al composite is enhanced by addition of Si and SiC while addition of ES lowers thermal conductivity. As expect, ES is a ceramic and so has very low thermal conductivity. Consequently, 20 wt.% ES is expected to significantly lower the thermal conductivity of both Gr–Al + 20% Si + 20 wt.%ES and Gr–Al + 20%SiC + 20 wt.%ES composites. For thermal management, Gr–Al + 20%Si is therefore preferable.

Analysis of fracture surfaces

The fractured surfaces of the sintered Gr–Al samples reinforced with different fillers are shown in Figure 9. Generally, uneven large dimples/cups are observed on the surfaces indicating that significant necking and shear preceded failure. Also, the dull appearance of the surfaces point to the ductile nature of the materials. A few undeformed particles were also observed. It appears that less number of dimples is present in Gr–Al + 20%SiC + 20 wt.%ES composite (Figure 9c) compared to others. This can be correlated to the fact that this composite has the highest microhardness value (see Figure 6) which is expected to reduce elongation prior to deformation.

Conclusions

This paper reports the influence of addition of ES particles on the morphology, displacement rate, electrical and thermal conductivity, R.D. and phase distribution of Gr–Al-based composites. Our results indicated enhanced microhardness value and decreased CTE compared to the base Gr–Al. Also, the R.D. decreased while porosity increased. In all, this study has shown that these properties of Gr–Al-based composites can be influenced positively by addition of ESs.

Declaration of Conflicting Interests

The author(s) declared no potential conflicts of interest with respect to the research, authorship, and/or publication of this article.

Funding

The author(s) received no financial support for the research, authorship, and/or publication of this article.

ORCID iD

TB Asafa  <https://orcid.org/0000-0001-6586-5193>

References

- Huang Y, Su Y, Li S, et al. Fabrication of graphite film/aluminum composites by vacuum hot pressing: process optimization and thermal conductivity. *Compos Part B* 2016; 107: 43–50.
- Durowoju MO, et al. Effect of micron and nano-sized ZrB₂ addition on the microstructure and properties of spark plasma sintered graphite–aluminum hybrid composite. *J Mater Sci Mater Electron* 2016; 27: 4672–4688.
- Karoly Z, Balazsi C, Petrick A, et al. Hybrid aluminum matrix composites prepared by spark plasma sintering (sps). *Eur Bull* 2014; 3: 247.
- Zhang L, et al. Aluminum/graphene composites with enhanced heat-dissipation properties by in-situ reduction of graphene oxide on aluminum particles. *J Alloys Compd* 2018; 748: 854–860.
- Rashad M, Pan F, Tang A, et al. Effect of graphene nanoplatelets addition on mechanical properties of pure aluminum using a semi-powder method. *Prog Nat Sci Mater Int* 2014; 24: 101–108.
- Li G and Xiong B. Effects of graphene content on microstructures and tensile property of graphene-nanosheets/aluminum composites. *J Alloys Compd* 2017; 697: 31–36.
- Durowoju MO, Sadiku ER, Diouf S, et al. Spark plasma sintering of graphite–aluminum powder reinforced with SiC/Si particles. *Powder Technol* 2015; 284: 504–513.
- Toro P, Quijad R, Yazdani-Pedram M, et al. Eggshell a new bio-filler for polypropylene composites. *Mater Lett* 2007; 61: 4347–4350.
- Hincke MT, Nys Y, Gautron J, et al. The eggshell: structure, composition and mineralization. 2012; 17: 1266–1280.
- Hassan SB and Aigbodion VS. Effects of eggshell on the microstructures and properties of Al–Cu–Mg/eggshell particulate composites. *J King Saud Univ – Eng Sci* 2015; 27: 49–56.
- Chaithanyasai A, Vakchore PR and Umasankar V. The micro structural and mechanical property study of effects of egg shell particles on the aluminum 6061. *Procedia Eng* 2014; 97: 961–967.
- Shuhadah S and Supri AG. LDPE-isophthalic acid-modified egg shell powder. *J Phys Sci* 2009; 20: 87–98.
- Sudharsan B and Kumar ML. The mechanical behaviour of eggshell and coconut coir reinforced composites. *International Journal of Engineering Trends and Technology (IJETT)* 2014; 18: 9–13.
- Hamdi WJ and Habubi NF. Preparation of epoxy chicken eggshell composite as thermal insulation. 2017; 1–5. DOI: 10.1007/s41779-017-0145-4.
- Murugan S, Munusamy Y, Muniandy M, et al. Development of HDPE-modified eggshell composite. 2016; 1–8. DOI: 10.1002/pc.
- Hassan SB, Aigbodion VS and Patrick SN. Tribology in industry development of polyester/eggshell particulate composites. *International Journal of Engineering Trends and Technology (IJETT)* 2012; 34: 217–225.
- Huang J-L and Nayak PK. Strengthening alumina ceramic matrix nanocomposites using spark plasma sintering. In: Narottam P Bansal and JP Singh (eds) *Advances in ceramic matrix composites*. Vol. 2. UK: Woodhead Publishing Limited, 2014, pp.218–234.
- Raichenko AI. Theory of metal powder sintering by an electric-pulse discharge. *Sov Powder Met Met Ceram* 1985; 24: 26–30.
- Maca K, Pouchly V and Boccaccini AR. Sintering densification curve – a practical approach for its construction from dilatometric shrinkage data. *Sci Sinter* 2008; 40: 117.
- Largiller G, Dong L, Bouvard D, et al. Constitutive modeling of the behavior of cermet compacts during reaction sintering. *Powder Technol* 2011; 208: 496.
- Olivier G, et al. Field-assisted sintering technology. *Adv Eng Mater* 2014; 95: 425.

22. Zhou C, et al. Fabrication, interface characterization and modeling of oriented graphite flakes/Si/Al composites for thermal management applications. *Mater Des* 2014; 63: 719–728.
23. Fukushima H. High thermal conductivity graphite particles dispersed composite and its production method 2005, US, Patent US7851055B2, Assigned to Hitachi Metals Ltd.
24. Jo S and Kang S. Effect of zinc-borate glass addition on the thermal properties of the cordierite/ Al_2O_3 composites containing nano-sized spinel crystal. *J Nanosci Nanotechnol* 2013; 13: 7675–7679.
25. Diouf S and Molinari A. Densification mechanisms in spark plasma sintering: effect of particle size and pressure. *Powder Technol* 2012; 221: 220–227.
26. Rodríguez A, Guerrero SA, Sanchez J, et al. Pressure infiltration of Al–12wt.% Si–X (X = Cu, Ti, Mg) alloys into graphite particle performs. *Acta Mater* 2006; 54: 1821.
27. Shehata F, Elmahallawy N, Arab M, et al. Equal channel angular pressing of Al–SiC composites fabricated by stir casting. *Open J Met* 2013; 3: 326–333.
28. Chaithanyasai A, Vakchorea PR and Umasankara V. The micro structural and mechanical property study of effects of eggshell particles on the aluminum 6061. *Procedia Eng* 2014; 97: 961–967.
29. Hussein SI, Abd-Elnaiem AM, Asafa TB, et al. Effect of incorporation of conductive fillers on mechanical properties and thermal conductivity of epoxy resin composite. *Appl Phys A Mater Sci Process* 2018; 124: 475.
30. Serway RA. *Principles of physics*. 2nd ed. Fort Worth, Texas; London: Saunders College Pub, 1998, p.602.
31. Dhanoa PS, Puri VM and Anantheswaran RC. Thermal and mechanical properties of eggshell under different treatment. *Trans ASAE* 1996; 39: 999–1004.